Journal of Nuclear Materials 382 (2008) 77–90

Contents lists available at ScienceDirect

Journal of Nuclear Materials

journal homepage: www.elsevier.com/locate/jnucmat

Mean field rate theory and object kinetic Monte Carlo: A comparison of kinetic models

R.E. Stoller [a,*], S.I. Golubov [b], C. Domain [c], C.S. Becquart [d]

[a] Materials Science and Technology Division, Oak Ridge National Laboratory, P.O. Box 2008, Oak Ridge, TN 37831-6158, USA
[b] Center for Materials Processing, University of Tennessee, East Stadium Hall, Knoxville, TN 37996-0750, USA
[c] EDF-R&D Département MMC, Les Renardières, F-77818 Moret sur Loing Cédex, France
[d] Laboratoire de Métallurgie Physique et Génie des Matériaux, UMR 8517, Université Lille-1, F-59655 Villeneuve d'Ascq Cédex, France

A B S T R A C T

Multiscale modeling schemes encompass models from the atomistic to the continuum scale. Phenomena at the mesoscale have typically been simulated using models based on reaction rate theory, such as mean field rate theory (MFRT) or Monte Carlo. These mesoscale models are appropriate for application to problems that involve intermediate-length scales, and timescales from those characteristic of diffusion to long-term microstructural evolution (~μs to years). Although the MFRT and Monte Carlo models can be used simulate the same phenomena, some of the details are handled quite differently in the two approaches. Models employing the rate theory have been extensively used to describe radiation-induced phenomena such as void swelling and irradiation creep. The primary approximations in such models are time and spatial averaging of the radiation damage source term, and spatial averaging of the microstructure into an effective medium. Kinetic Monte Carlo models can account for these spatial and temporal correlations; their primary limitation is the computational burden, which is related to the size of the simulation cell. Even with modern computers, the maximum simulation cell size and the maximum dose (typically much less than 1 dpa) that can be simulated are limited. In contrast, even very detailed MFRT models can simulate microstructural evolution for doses up 100 dpa or greater in clock times that are relatively short. Within the context of the effective medium, essentially any defect density can be simulated. A direct comparison of MFRT and object kinetic MC simulations has been made in the domain of point defect cluster dynamics modeling, which is relevant to the evolution (both nucleation and growth) of radiation-induced defect structures. Overall, the agreement between the two methods is best for irradiation conditions that produce a high density of defects (lower temperature and higher displacement rate) and for materials that have a relatively high density of fixed sinks such as dislocations.

1. Introduction

Developing an adequate quantitative understanding of the changes in the physical and mechanical properties of materials that occur during thermal aging or under irradiation requires a model capable of describing the formation and growth of point defect and solute clusters through all stages of cluster evolution, from their nucleation to growth and coarsening. This so-called cluster dynamics behavior has been extensively investigated by two alternate implementations of reaction rate theory: the mean field rate theory (MFRT) and object kinetic Monte Carlo (OKMC). The MFRT approach is used so extensively that the distinction between this specific implementation and the underlying reaction rate theory is often forgotten or neglected. In principle, MFRT and OKMC should predict essentially the same behavior when used to solve the same problem. However, this equivalence has not been demonstrated in such a specific case. The purpose of the present study was to benchmark these two approaches against one another using a series of well-posed computational problems. The intent was to either verify that the expected equivalent predictions were obtained, or to determine regimes for which equivalence was not obtained. In the latter case, an effort was made to explain any differences that were observed. Because the study was focused on benchmarking and comparing the two methods, the simulations generally involved idealized conditions or in some cases non-physical parameter choices. As a result, no direct comparison with experimental data was possible. Following the Introduction, a brief, self-contained description of both the computational methods is provided in Section 2. An extensive comparison of the predictions obtained from the models on the sample problems is given in Section 3. This is followed by a short Discussion and Summary.

The evolution of a random spatial distribution of defect clusters can be described in terms of a defect size distribution function

* Corresponding author. Tel.: +1 865 576 7886.
E-mail address: rkn@ornl.gov (R.E. Stoller).

0022-3115/$ - see front matter © 2008 Elsevier B.V. All rights reserved.
doi:10.1016/j.jnucmat.2008.08.047

(SDF) in the framework of the mean field approximation [1]. Evolution of this SDF can be accounted for in the context of a MFRT model through the use of a Master Equation (ME) that describes both growth and dissolution of the clusters due to reactions with mobile defects (or solutes), thermal emission of these same species, and cluster coalescence if the clusters are mobile. The relevant physical processes require accounting for clusters containing a very large number of point defects or atoms ($>10^6$), particularly for high irradiation doses or long ageing times. An explicit discretization of the ME leads to a system of coupled differential equations in which time is an explicit variable. The number of equations is the same as the number of point defects (and/or solutes) in the largest possible cluster. Numerical integration of such a system is feasible on modern computers, but such calculations are overly time consuming. Most practicable solutions to the ME by numerical methods employ some grouping procedure to significantly reduce the number of equations [2–7].

The OKMC technique provides another method for calculating the evolution of the cluster SDF. This method has become practicable during the last decade because of progress in computer technology. In the framework of OKMC, each point defect or defect cluster is treated as an object located in a specific position in a simulation cell of a given volume. Irradiation is simulated by introducing new point defects or defect clusters at discrete times and in specific locations in the box, and evolution occurs as the various objects migrate and participate in a series of predefined reactions with other objects. Each object type has associated properties, such as size, reaction radius, and, if mobile, jump frequency and activation energy for migration. The reaction probabilities for various physical transition mechanisms, such as migration jump rates and the emission rate of point defects from larger defects or traps, are calculated based on Arrhenius frequencies for thermally activated events. The Monte Carlo algorithm [8] is used at each step to select the event that is going to take place based on the corresponding probabilities. After a given event is chosen, the time is increased according to an algorithm that depends on the jump frequencies for all the possible events in the system.

One advantage of the MFRT approach is that there are essentially no limits to the density or size of the clusters when calculating their evolution, providing the opportunity to compare with a broad range of experimental observations. However, the spatial and temporal correlations in defect production are not accounted for, which may in some cases lead to a loss of specific information. OKMC models can account for these spatial and temporal correlations; their primary limitation is related to the size of the simulation cell. To maintain a reasonable simulation time, the practicable box size is typically a cube with an edge length on the order of 100 nm. This limits the total cluster number density that may be obtained in this method. For example, if there is only one cluster in a 100-nm × 100-nm × 100-nm simulation cell, the corresponding cluster number density is 10^{21} m^{-3}. This is an intermediate to high defect density for many relevant irradiated materials, and no lower cluster density can be treated by OKMC in a box of this size. Even for the relatively high defect density of 10^{22} m^{-3}, the number of clusters in such a simulation cell would only be 10, which may not be enough to provide a good statistical simulation of defect cluster evolution. Another problem with statistics may arise when simulating clusters that are not stable in a certain size range, that is, when cluster nucleation requires reaching a certain critical size at which they become stable enough to be able grow continuously. Such nucleation is possible due to fluctuations in the cluster growth and resolution processes and will be properly calculated by OKMC only if the density is sufficiently high to maintain such fluctuations.

Thus, both the MFRT and OKMC have advantages and limitations based on the underlying nature of the techniques; the major features of these models are briefly summarized in Table 1. Because the two techniques simply represent different mathematical methods for solving a given problem, they should provide similar results for well designed sample problems. A systematic application of the two methods will determine if they produce consistent results, or whether there are problems for which one method is preferable to the other. This is the main objective of the present study. Because the MFRT approach has been well-established by broad use during the last few decades, the approach taken here was to use MFRT calculations as a reference point to evaluate the predictions of the OKMC method for several different types of simulations. The specific MFRT and OKMC models used for this comparison are discussed in the next section.

2. Description of models

The comparison of the two approaches is more straightforward if restricted to a particular case. This investigation is focused on the evolution of the SDF of vacancy and self-interstitial clusters in a pure metal under irradiation with a constant network dislocation density as the only fixed sink. In the following discussion, the term void is used in a generic way to refer to a vacancy cluster of any size. The formulated model makes use of the following assumptions:

1. The primary damage is produced either (a) in the form of Frenkel pair, that is, only single vacancies and self-interstitial atoms (SIAs); or (b) Frenkel pair plus small clusters of either vacancies or SIAs typical of those generated by displacement cascades.
2. The point defects diffuse by three-dimensional (3-D) random walk.
3. The nucleation of vacancy and SIA clusters proceeds via a homogeneous mechanism, that is due to monodefect + monodefect = di-defect in the case of 1(a), or by both homogeneous and in-cascade clustering mechanisms at the same time for 1(b).
4. Vacancy clusters are treated as spherical voids that are neutral sinks for point defects; thermal emission of vacancies is determined by a size-dependent binding energy.
5. SIA clusters are treated as 3-D spherical clusters, with a preference (bias) for absorbing SIAs relative to vacancies, and are stable against thermal SIA emission;

Table 1
Comparison of MFRT and OKMC methods

Feature or treatment of variable	MFRT	OKMC
Solution method	Deterministic	Stochastic
Time	Explicit variable	Inferred from possible processes and reaction rates
Space	Homogeneous effective medium[a]	Full spatial dependence
Defect production	Time and space-averaged[a]	Discrete in time and space
Sink strength	Explicit analytical expression	Inferred from fate of point defects
Defect or sink density	Essentially unlimited	Computationally limited by simulation cell size, that is: $N_{min} \geqslant 1$/(box volume)

[a] Partial corrections to the typical MFRT approximations are possible, including multiregion MFRT models to account for spatial dependence in a limited way and the use of a so-called cascade diffusion model [9] to treat the time dependence of primary damage formation.

6. Edge dislocations are a fixed matrix sink with a preference (bias) for SIAs that is the same as the SIA clusters; and
7. The vacancy and SIA clusters are immobile.

These assumptions are only used for simplification and do not lead to any restrictions in comparing the two methods. For example, a planar loop is a better approximation of SIA cluster geometry. The spherical geometry was used here to simplify the MFRT-OKMC comparison. However, to provide a self-contained description of the MFRT sink strengths, the relevant equations are first presented for both planar and spherical sinks. Neglecting the mobility of small vacancy of SIA clusters will increase the density of clusters in both models. Higher cluster densities improve the statistics in the OKMC model as will be discussed below.

2.1. Mean field rate theory model

2.1.1. Form of master equation

Based on the assumptions listed above, the SDF of voids, $f_{vcl}(x,t)$, and SIA clusters, $f_{icl}(x,t)$, can be described by the following pair of master equations, in which x is the number of point defects in the cluster [3,10]:

$$\frac{\partial f_{vcl}(x,t)}{\partial t} = K_{vcl}(x) + J_{vcl}(x-1,t) - J_{vcl}(x,t) \tag{1a}$$

$$\frac{\partial f_{icl}(x,t)}{\partial t} = K_{icl}(x) + J_{icl}(x-1,t) - J_{icl}(x,t), \tag{1b}$$

$$\sum_{x=2}^{\infty} xK_{vcl}(x) = \varepsilon_{vcl} G_{\mathrm{NRT}}(1-\varepsilon_r), \quad \sum_{x=2}^{\infty} xK_{icl}(x) = \varepsilon_{icl} G_{\mathrm{NRT}}(1-\varepsilon_r). \tag{1c}$$

The $K_{vcl}(x)$, $K_{icl}(x)$ are the rates of in-cascade generation of voids and SIA loops, respectively, ε_r is the fraction of Frenkel pair that recombines during the cascade cooling; ε_{vcl}, ε_{icl} are the in-cascade clustering fractions for vacancies and SIAs, respectively; G_{NRT} is the NRT Frenkel pair generation rate; and $J_{vcl}(x,t)$, $J_{icl}(x,t)$ are the void and SIA loop fluxes in cluster size space, respectively:

$$J_{vcl}(x,t) = P_{vcl}(x,t) f_{vcl}(x,t) - Q_{vcl}(x+1,t) f_{vcl}(x+1,t), \tag{2a}$$

$$J_{icl}(x,t) = P_{icl}(x,t) f_{icl}(x,t) - Q_{icl}(x+1,t) f_{icl}(x+1,t). \tag{2b}$$

In Eqs. (2), $P_{vcl}(x,t)$ and $P_{icl}(x,t)$ are the rates of vacancy absorption by a void and SIA absorption by a SIA cluster, respectively; $Q_{vcl}(x,t)$ is the sum of the rates of SIA absorption and vacancy emission from a void, and $Q_{icl}(x,t)$ the rate of vacancy absorption by a SIA cluster. These rates depend on the cluster concentration and the diffusion properties of the mobile defects, that is, vacancies and SIAs. In the case of 3-D diffusion of point defects to voids and SIA loops, the rates take the following form [3,10]:

$$P_{vcl}(x) = w_{vcl} x^{1/3} D_v C_v(t), \tag{3a}$$

$$Q_{vcl}(x) = w_{vcl} x^{1/3} [D_i C_i + D_v \exp(-E_v^b(x)/kT)] = Q_{vcl}^i(x) + Q_{vcl}^v(x), \tag{3b}$$

$$P_{icl}(x) = Z_i^l w_{icl} x^{1/2} D_i C_i(t), \tag{4a}$$

$$Q_{icl}(x) = Z_v^l w_{icl} x^{1/2} D_v C_v(t), \tag{4b}$$

$$w_{vcl} = \left(\frac{48\pi^2}{\Omega^2}\right)^{1/3}, w_{icl} = \left(\frac{4\pi}{\Omega b}\right)^{1/2}. \tag{5}$$

$C_{i,v}(t)$ and $D_{i,v}$ are the concentrations and diffusion coefficients, respectively, of vacancies (subscript v) and SIAs (subscript i), Z_v^l, Z_i^l are the dislocation loop capture efficiencies for vacancies and SIAs, $E_v^b(x)$ is the binding energy of a vacancy to a vacancy cluster of size x, k_B is Boltzmann's constant, T is the absolute temperature, Ω is the atomic volume, and b is the magnitude of the SIA loop Burgers vector. For the case in which the dislocation loops are treated as 3-D clusters, which is used in the OKMC calculations, the parameter w_{icl} has to be replaced by w_{vcl} and $x^{1/2}$ replaced by $x^{1/3}$ in Eqs. (4a) and (4b).

Note that if the SDFs described by Eqs. (1a) and (1b) are written in x-space, the cluster densities are dimensionless. That is, the total density of clusters, $N_{vcl,icl} = \sum_{x=2}^{\infty} f_{vcl,icl}(x)$, has the units [1/atom]. The capture efficiencies used in Eqs. (3) and (4) have dimensions of [m^{-2}], and the cluster sink strengths, which are given by

$$k_{vcl}^2 = \sum_{x=2}^{\infty} P_{vcl}(x) f_{vcl}(x) \equiv w_{vcl} \sum_{x=2}^{\infty} x^{1/3} f_{vcl}(x), \tag{6a}$$

$$k_{icl(v,i)}^2 = \sum_{x=2}^{\infty} P_{icl(v,i)}(x) f_{icl}(x) \equiv Z_{v,i}^{icl} w_{icl} \sum_{x=2}^{\infty} x^{1/2} f_{icl}(x), \tag{6b}$$

also have the dimensionality of [m^{-2}]. For the purpose of comparing the results obtained by the MFRT and OKMC techniques, it will be useful to show that the sink strengths given by Eqs. (6) are equivalent to those that are normally used in the mean size approximation in MFRT models:

$$k_{vcl}^2 = 4\pi < R_{vcl} > N_{vcl}, \tag{7a}$$

$$k_{icl(v,i)}^2 = 2\pi Z_{v,i}^{icl} < R_{icl} > N_{icl}, \tag{7b}$$

which describe damage accumulation in the form of planar and spherical sinks using the loop capture efficiency for vacancies and interstitials, $Z_{v,i}^{icl}$, the mean cluster radii <R_{vcl}> and <R_{icl}>, and the corresponding total number densities N_{vcl} and N_{icl} with units of m and m^{-3}, respectively. To show this, the SDF can be calculated in the domain where the size of a cluster is defined by its radius, r, instead of x. The SDFs can be calculated by taking into account that a sum of the SDF over all sizes in any phase space used for the ME has to be equal to the total number of clusters, N_{tot}. Replacing the sums with integrals, the total number density of the clusters in the case under consideration may be written as

$$N_{\mathrm{tot}} = \int_{x=2}^{\infty} f(x)\mathrm{d}x \equiv \int_{R=R_{\min}}^{\infty} f(R)\mathrm{d}R. \tag{8}$$

The two integrals in Eq. (8) can be equal to each other if

$$f(x)\mathrm{d}x = f(R)\mathrm{d}R. \tag{9}$$

Taking into account that the radii of voids, R_{vcl}, and loops, R_{icl}, and the total number of defects in the clusters, x_{vcl}, x_{icl}, are related to each other as follows

$$\frac{4\pi}{3} R_{vcl}^3 = x_{vcl}\Omega, \pi R_{icl}^2 b = x_{icl}\Omega, \tag{10}$$

and using Eq. (9) the functions $f_{vcl}(R_{vcl})$ and $f_{icl}(R_{icl})$ can be easily calculated

$$f_{vcl}(R_{vcl}) = f_{vcl}(x)\left(\frac{36\pi}{\Omega}\right)^{1/3} x^{2/3},$$

$$f_{icl}(R_{icl}) = f_{icl}(x)\left(\frac{4\pi b}{\Omega}\right)^{1/2} x^{1/2}. \tag{11}$$

Note that dimensionality of the functions $f_{vcl}(R_v), f_{icl}(R_i)$ is $\left[\frac{1}{m}\ \frac{1}{\mathrm{atom}}\right]$ On the other hand the SDFs in r-space are normally presented as a number of clusters per unit volume. This can be obtained by dividing the right-hand sides of Eqs. (11) by the atomic volume, Ω, i.e., $F_{vcl,icl}(R_{vcl,icl}) = \frac{1}{\Omega} f_{vcl,icl}(R_{vcl,icl})$. Here the capital F is used to distinguish the SDFs with dimensions (m^{-4}) from the SDFs $f_v(R_v), f_i(R_i)$. Using Eqs. (10) and (11) and replacing the sums in Eq. (6) by the corresponding integrals one can easily find that

$$k_{vcl}^2 = \left(\frac{48\pi^2}{\Omega^2}\right)^{1/3} \int_{x=2}^{\infty} x^{1/3} f_{vcl}(x)\mathrm{d}x = 4\pi \int_{R_{vcl,\min}}^{\infty} R_{vcl} F_{vcl}(R_{vcl})\mathrm{d}R_{vcl} \equiv 4\pi < R_{vcl} > N_{vcl}, \tag{12a}$$

$$k^2_{icl(v,i)} = Z^{icl}_{v,i}\left(\frac{4\pi}{\Omega b}\right)^{1/2}\int_{x=2}^{\infty} x^{1/2} f_{icl}(x) = 2\pi Z^{icl}_{v,i}\int_{R_{i,\min}}^{\infty} R_{icl}F_{icl}(R_{icl})\mathrm{d}R_{icl} \equiv 2\pi Z^{icl}_{v,i} < R_{icl} > N_{icl}. \quad (12b)$$

where

$$\langle R_{vcl}\rangle = \frac{\int_{R_{v,\min}}^{\infty} R_{vcl}F_{vcl}(R_{vcl})\mathrm{d}R_{vcl}}{\int_{R_{v,\min}}^{\infty} F_{vcl}(R_{vcl})\mathrm{d}R_{vcl}}$$
$$\langle R_{icl}\rangle = \frac{\int_{R_{i,\min}}^{\infty} R_{icl}F_{icl}(R_{icl})\mathrm{d}R_{icl}}{\int_{R_{i,\min}}^{\infty} F_{icl}(R_{icl})\mathrm{d}R_{icl}}. \quad (13)$$

Although the integral of the SDFs shown in Eq. (7) has the same value for either phase space, the difference in dimensionality means the two SDF have quite different shapes in r- or x-space. These two are compared in Fig. 1, where the void SDFs obtained using the MFRT for a specific case are plotted in both r- and x-space. Although use of the x-space description may be more convenient for the purpose of calculations, the r-space SDF is more appropriate for comparing with experimental observations such as TEM measurements.

2.1.2. Initial and boundary conditions

The initial and boundary conditions for void and SIA loop SDFs, and the point defect concentrations are described as follows:

$$f_{vcl}(x, t=0) = C_{v0}\delta(x-1), \quad f_{icl}(x, t=0) = 0, \quad (x \geqslant 1), \quad (14a)$$
$$f_{vcl}(x=1, t) = C_v(t), \quad f_{icl}(x=1, t) = C_i(t), \quad (14b)$$
$$f_{vcl}(x=\infty, t) = f_{icl}(x=\infty, t) = 0, \quad (14c)$$
$$C_v(t=0) = C_{v0}C_i(t=0) = 0, \quad (14d)$$

where $C_{v0}\exp\left(-\frac{E^f_v}{k_BT}\right)$ is the thermal equilibrium vacancy concentration, E^f_v is the vacancy formation energy, and $\delta(x)$ is the Kronneker delta.

2.1.3. Equations for point defect concentrations

To complete the system of equations, we must add equations for the evolution of the vacancies, C_v, and SIAs, C_i, which are given by [5]:

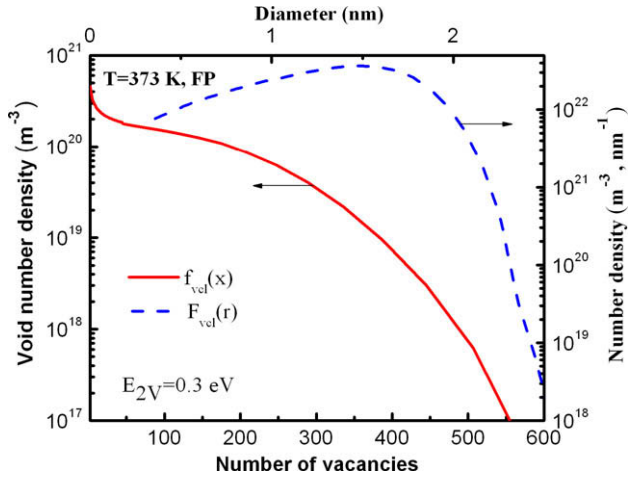

Fig. 1. Void size distribution function calculated for the case of $E_{2v} = 0.3$: $f_{vcl}(x)$ in phase space x (x = number of vacancies), and $F_{vcl}(d)$ in phase space d (d = void diameter).

$$\frac{\mathrm{d}C_v(t)}{\mathrm{d}t} = G_{\mathrm{NRT}}(1-\varepsilon_r)(1-\varepsilon_{vcl}) - \left[\mu_R D_i C_i(t) C_v(t) + Z^d_v \rho D_v (C_v(t) - C_{v0}) + \sum_{x=2}^{x=\infty} P_{icl}(x) f_{icl}(x,t)\right] - [P_{vcl}(1) f_{vcl}(1,t) - (Q^v_{vcl}(2) + Q^i_{vcl}(x)) f_{vcl}(2,t)] - \sum_{x=1}^{x=\infty}(P_{vcl}(x) f_{vcl}(x,t) - Q^v_{vcl}(x+1) f_{vcl}(x+1,t)), \quad (15)$$

$$\frac{\mathrm{d}C_i(t)}{\mathrm{d}t} = G_{\mathrm{NRT}}(1-\varepsilon_r)(1-\varepsilon_{icl}) - \left[\mu_R D_i C_i(t) C_v(t) + Z^d_i \rho D_i C_i + \sum_{x=1}^{x=\infty} P_{icl}(x) f_{icl}(x,t)\right] - [P_{icl}(1) f_{icl}(1,t) - Q_{icl}(2) f_{icl}(2,t)] - \sum_{x=1}^{x=\infty} Q^i_{vcl}(x+1) f_{vcl}(x+1,t), \quad (16)$$

where G_{NRT} is the point defect generation rate, μ_R is the recombination coefficient, ρ is the dislocation density, and Z^d_v, Z^d_i are the dislocation capture efficiencies for vacancies and SIAs, respectively (here Z^d_v is set equal to 1.0). The first term on the right-hand side of Eqs. (15) and (16) is the generation rate of mobile point defects, and the second term includes the point defect annihilation rates by recombination, reactions, and absorption by dislocations, and the SIA clusters. The third term accounts for the fact that a reaction between mobile monomers eliminates both of them, and reactions between mobile monomers and a dimer of the opposite species generates a mobile monomer of the same species as the dimer, i.e., vacancy + di-interstitial = interstitial. The last term is the point defect capture rate by voids.

Eqs. (1)–(4), (15) and (16) comprise a large system of coupled nonlinear differential equations and, in the general case, can be only solved by numerical methods. For realistic sizes of voids and SIA clusters, the system size can exceed 10^6 equations, requiring that practicable solution of this system will require some grouping procedure to minimize the number of equations. This amounts to approximating the continuous SDF as a histogram [2–7]. In the present work the grouping method developed by Golubov et al. [5] was used.

2.2. Object kinetic Monte Carlo model

2.2.1. Thermally activated processes

The general features of the OKMC code used in the present work, LAKIMOCA, are described in Ref. [11]. The model treats radiation-produced defects (vacancies, SIAs, and clusters thereof) as objects that have specific reaction volumes and that are located in particular positions in the simulation box. Each object can migrate and participate in a series of predefined reactions. The probabilities for physical transition mechanisms, which are basically migration jumps and emission from larger defects or from traps, are calculated in terms of Arrhenius frequencies for thermally activated events, $\Gamma_i = \nu_i \exp\left(-\frac{E_{a,i}}{k_BT}\right)$, where ν_i is the attempt frequency (prefactor) for event i, and $E_{a,i}$ is the corresponding activation energy. The Monte Carlo algorithm [8] is used at each step to select the event that is going to take place, based on the corresponding probabilities. After a certain event is chosen, time is increased according to the residence time algorithm, $\Delta\tau = \left(\sum_{i=1}^{N^{\mathrm{th}}_e}\Gamma_i + \sum_{j=1}^{N^{\mathrm{ext}}_e} P_j\right)^{-1}$ Ref. [12], where the P_j are the probabilities of external events, such as the appearance of a cascade or of isolated Frenkel pair produced by impinging particles. The choice of

this expression is in the long-term equivalent to choosing $\Delta\tau' = -\ln R^* \Delta\tau$, where R is a random number between 0 and 1 Ref. [13].

2.2.2. Sink Strengths in the OKMC

In addition, the OKMC model includes non-thermally activated events, such as the annihilation of a defect after encountering either a defect of opposite nature (i.e., a SIA encountering a vacancy) or a sink, as well aggregation, either by adding a point-defect to a cluster or by forming a complex between a defect and a trap for it. These events occur only on the basis of geometrical considerations (overlap of reaction volumes) and do not participate in defining the progression of time. It is possible to introduce different classes of immobile traps and sinks, characterized by specific geometrical shapes (spheres, infinite cylinders, surfaces etc.) suitable for mimicking voids and other defects such as dislocations and grain boundaries.

In the present work, the OKMC technique is used to simulate damage accumulation according to the model formulated above. A bcc iron lattice containing edge dislocations is simulated, with the evolution of two types of point defect clusters, voids and SIA loops. To simplify the calculations, both types of defect clusters are treated as spherical absorbers. The only difference between the vacancy clusters and the SIA loops is that the first ones are described as neutral sinks, whereas the second are considered to be biased, i.e. having preference for absorption of SIAs. Thus, instead of using Eq. (6b), the sink strength of the SIA clusters is given by

$$k^2_{icl(v,i)} = Z^{icl}_{v,i} w_v \sum_{x=2}^{\infty} x^{1/3} f_i(x) \equiv 4\pi Z^{icl}_{v,i} < R_i > N_i (Z^{icl}_v = 1, Z^{icl}_i > 1). \tag{17}$$

The bias of the SIA clusters is equal to $p_l = (Z^{icl}_i - Z^{icl}_v)/Z^{icl}_v \equiv Z^{icl}_i - 1$ and in the following calculations is chosen to be equal of that for the dislocations, that is, $Z^{icl}_i = Z^d_i$. Note that such an approach for the shape of SIA clusters in the following calculations is quite reasonable because the sink strengths of small spherical clusters and that of dislocation loops are similar when the cluster size is not large. Using Eqs. (6) one can find that the ratio of the sink strengths is given by

$$\frac{(k^2_{icl})_{\text{spherical}}}{(k^2_{icl})_{\text{loop}}} \approx (\pi 3^{3/2})^{1/6} x^{-1/6} = 1.592 x^{-1/6}, \tag{18}$$

that is, it only weakly depends on the number of defects in the cluster (it varies within a factor of 2 when x varies in a range from 2 to 10^4). This size range matches well the calculations presented in this work since the highest irradiation dose used in the calculations is rather small (10^{-2} dpa).

When the sink strength of small clusters is accounted for in the OKMC, a measurable difference is observed between the MFRT and OKMC. This arises from the discrete spatial description of point defect absorption in the OKMC. In the case of the MFRT, the equivalent radius of a cluster containing any number of point defects can be calculated using Eq. (10), and this radius determines the sink strength, which is essentially the probability of the cluster absorbing a mobile point defect in that model. However, in the OKMC model, a cluster of X point defects occupies X lattice sites. Point defect absorption occurs when a mobile point defect arrives at an adjacent lattice site. For relatively large clusters the OKMC and MFRT reaction probabilities or sink strengths are nearly the same because the larger clusters are more nearly spherical. However, the equivalent radius given by Eq. (10) overestimates the reaction rate for small clusters. This is illustrated in Fig. 2, in which the sink strength obtained by the two models is shown for vacancy clusters containing up to 500 vacancies (equivalent radius of 1.12 nm). Note that the acronym RT in this and subsequent figures

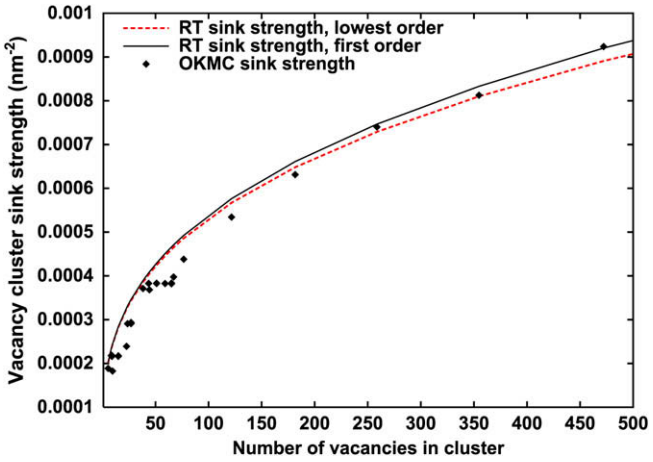

Fig. 2. Comparison of vacancy cluster sink strength obtained in OKMC simulations (discrete points) and the analytical expression applied in the MFRT (lines). The dashed line is the lowest order sink strength, which is valid for small sink volume fractions, and the solid line includes the first-order sink strength correction factor [14].

is an abbreviation for MFRT. The discrete points were obtained by OKMC simulations in which point defect absorption was computed for vacancy clusters of the indicated size. The lines indicate MFRT sink strengths computed using the equivalent radius from Eq. (10). The dashed line is obtained using the lowest order expression for the sink strength, Eq. (7a), and the solid line is obtained when the first-order correction term is included to account for multiple sink effects [14]. This multiple sink correction is implicitly accounted for in the OKMC method. The impact of this difference in sink strength will be discussed further when the results are presented in Section 3.

More than one approach could be followed to simulate the sink strength of dislocations in OKMC. One possible method is the direct introduction of an absorbing cylinder of a certain length, L_d, corresponding to the desired dislocation density, ρ, and with specified capture efficiencies for point defects. In this case, one may expect to reproduce the sink strength given in Eqs. (15) and (16) with the efficiencies $Z^d_{v,i} = \frac{2\pi}{\ln}\left[(kR_{cv,ci})^{-1}\right]$, which leads to a dislocation bias to be equal to

$$p = \frac{Z^d_i - Z^d_v}{Z^d_v} = \frac{\ln(R_{di}/R_{dv})}{\ln\left[(kR_{di})^{-1}\right]}, \tag{19}$$

where r_{di}, r_{dv} are the cylinder capture radii for SIAs and vacancies, respectively, and $k = \sqrt{k^2}$ (where k^2 is the total sink strength in the crystal). This approach appears relatively intuitive and straightforward, but this is not the case. The first problem arises with choosing the cylinder length. To simulate a given dislocation density, ρ, the length of the cylinder has to be taken to be equal to $L_d = \rho V_{\text{box}}$, which may be too small or too large to fit conveniently in the simulation box, $L_{\text{box}} = V^{1/3}_{\text{box}}$. In addition, the dislocation density can vary by several orders of magnitude whereas the maximum box size is essentially fixed by computational limitations. As a result, such a cylinder may have its ends inside the simulation box and thus cannot reproduce the actual cylindrical symmetry of a dislocation. The impact of this on the dislocation sink strength requires further investigation, which is beyond the scope of the present work, and is not directly relevant to the comparison of the MFRT and OKMC methods. A second issue arises from the fact that the dislocation sink strength and corresponding bias depends on the total sink strength, k^2, see Eq. (19), which changes during the irradiation. Because of these issues, the alternate approach discussed in the next paragraph was used to simulate the dislocation sink density.

One way to avoid these complications is to simulate the dislocation sink by introducing another class of spherical absorber, which maintains the two main properties of dislocations as a sink for point defects: (a) a preference for SIA absorption, that is, maintain a constant dislocation bias and (b) maintain constant sink strength during irradiation. This may be achieved by introducing additional spherical absorbers with fixed density and size as follows:

$$k_{vd}^2 = 4\pi R_v^d N^d \equiv \rho, \tag{20a}$$

$$k_{id}^2 = 4\pi R_i^d N^d, (R_i^d > R_v^d). \tag{20b}$$

Thus choosing a specific capture radius for vacancies, R_v^d, the density of the absorbers, N^d, can be calculated from the first Eq. (25), $N^d = \frac{\rho}{4\pi R_v^d}$. The bias in the case is equal to

$$p = \frac{k_i^2 - k_v^2}{k_v^2} = \frac{R_i^d}{R_v^d} - 1, \tag{21}$$

i.e., it depends on the ratio of R_i^d/R_v^d only. Taking the ratio R_i^d/R_v^d to be equal to Z_i^d, one may expect that Eqs. (25) will reproduce the sink strength of dislocations with respect to their ability to capture point defects. Thus, Eqs. (25) and (21) permit calculating the absorber properties of dislocation at any given dislocation density and bias. The spherical absorbers used to simulate dislocations are randomly distributed in the simulation box, with capture radii of $R_v^d = 0.4$ nm, $R_i^d = 0.48$ nm for vacancies and SIAs, respectively.

An OKMC simulation cell size of $300 \times 300 \times 300$ lattice parameters was used in all the simulations discussed here. Given the lattice parameter of α-Fe (see Table 2), this leads to a volume equal to 6.423×10^{-22} m^3. As a result, the minimum density of any given object that can be obtained in the OKMC simulations is 1.56×10^{21} m^{-3}, that is, one per box volume. The impact of this limitation will be discussed below.

2.3. Material and irradiation parameters

To explore a range of irradiation phenomena and to help isolate the effects of different mechanisms, two types of irradiation conditions were considered:

1. Pure Frenkel pair production only, which is similar to electron irradiation, and
2. Cascade damage production, typical of heavy ion or neutron irradiation, in which 30% of the SIA and vacancies are produced in small clusters. The SIA clusters are distributed as follows: 14% di-, 12% tri-, 4% tetra-interstitials, while all of the vacancy clusters are initially of size six.

For the second case, two classes of cascade debris were considered in the OKMC simulations: (2a) normal cascades in which the point defects and defect clusters were spatially correlated as observed in atomistic simulations of cascade damage formation [15], and (2b) special 'random' cascades in which the spatial correlation was not preserved. Case (2b) is a better approximation of how the damage production is simulated in the MFRT model. The cascade efficiency, that is, the fraction of point defects that survive after the cascade cooling phase, is taken to be 0.4 for the cases of cascade damage production. When simulating Frenkel pair production, the cascade efficiency is essentially 1.0, so the damage rate was set to permit comparison with cascade damage results at the same effective displacement rate.

The binding energy of a vacancy with a void of size x is described using the capillarity model adjusted to a specific di-vacancy binding energy, E_{2v}. The general expression for the vacancy binding energy takes the following form:

$$E_v^b(x) = E_v^f + (E_{2v} - E_v^f)\left(\frac{x^{2/3} - (x-1)^{2/3}}{2^{2/3} - 1}\right). \tag{22}$$

The energy E_{2v} can be treated as a variable parameter to permit investigation of the stability of the vacancy clusters. A value of 0.2 eV was used in the OKMC and MFRT predictions presented below. The SIA clusters are treated as thermally stable. The nominal material and irradiation parameters are given in Table 2.

3. Results

A large number of figures will be presented to summarize the primary results. A consistent color scheme has been applied in each of the figures to aid the reader. The MFRT results are shown as red curves, and the OKMC as black symbols or curves. Parameters that were varied in the analysis are differentiated by different types of lines. In some cases, two sets of OKMC results are shown at a given dose. One is the instantaneous value at that dose, and the

Table 2
Material and irradiation parameters used in calculations

Temperature, T	373–523 K
Lattice parameter, a	0.2876 nm
Atomic volume, $\Omega = a^3/2$	1.189×10^{-29} m^3
Number of atoms in unit volume, $N = 1/\Omega$	8.407×10^{28} m^{-3}
Box volume of a cube of size 300a, V_{box}	6.423×10^{-22} m^3
Number of atoms in the box, $N_{box} = V_{box}/\Omega$	5.4×10^7
Number density equivalent to one cluster in, $N_{cl} = 1/V_{box}$	1.557×10^{21} m^{-3}
NRT displacement rate, G_{NRT}	4×10^{-7} to 4×10^{-5} dpa/s
Cascade survival efficiency, $(1-\varepsilon_r)$	0.40
Fraction of SIAs in cluster form, ε ($x = 2$, 3, and 4)	0.30
Fraction of voids in cluster form, ε_v ($x = 6$)	0.30
Recombination coefficient, $\mu_R = 4\pi(r_v + r_i)/\Omega$, ($r_v + r_i = 0.4466$ nm)	4.72×10^{20} m^{-2}
Attempt frequency, v	6.0×10^{12} s^{-1}
Vacancy diffusion coefficient, $D_v = D_{v0}\exp\left(-\frac{E_v^m}{kT}\right)$	6.02×10^{-8} m^2/s
Preexponential, $D_{v0} = \frac{1}{6} r^2 v \left(r = \frac{\sqrt{3}}{2} a\right)$	0.65 eV
Migration energy, E_v^m	
SIA diffusion coefficient, $D_i = D_{i0}\exp\left(-\frac{E_i^m}{kT}\right)$	6.02×10^{-8} m^2/s
Preexponential, $D_{i0} = \frac{1}{6} r^2 v$	0.30 eV
Migration energy, E_i^m	
Binding energy of di-vacancies, E_{2v}	0.2 eV
Capture efficiencies of dislocations and SIA clusters, $Z_v^{icl}, Z_i^{icl}, Z_v^d, Z_i^d$	1.0, 1.20
Dislocation density, ρ_d	3×10^{14} m^{-2}
Capture radii for 'dislocation' spherical absorbers, R_i^d, R_v^d	0.48 and 0.4 nm ($p = 0.2$)

other is the average value obtained from the value at that dose and values from the previous two timesteps and two subsequent timesteps. The preceding four timesteps were included in average values reported at the final dose. This helps to demonstrate the statistical nature of the OKMC results and permits results to be shown when the instantaneous value is less than the minimum of one per OKMC box volume. This minimum density is also indicated in some of the figures by a horizontal dashed blue line. The results presented include calculated values of vacancy and interstitial concentrations, vacancy and SIA cluster densities, the total number of vacancies and SIA accumulated in clusters, and the vacancy and SIA cluster size distributions. The net number of point defects accumulated in clusters is significant because it represents the volume change or swelling associated with the irradiation.

The simplest situation to simulate is that of only Frenkel pair production, with vacancy and interstitial cluster formation occurring only as a result of homogeneous nucleation. For this case, the three different sink behavior possibilities were considered:

1. No fixed sinks, vacancy and interstitial clusters can form by classical nucleation (diffusive encounters), the capture efficiency of both cluster types for mobile monovacancies and monointerstitials is the same, that is, there is no biased absorption.
2. The same as in 1 above, but SIA clusters have 20% interstitial bias; and
3. The same as in 2 above but the fixed (dislocation) sink with an interstitial bias of 20% and a density of 3×10^{14} m^{-2} is included.

Of these three, the last one is certainly most physically representative of the behavior expected in real materials. The use of the other two was intended to be a tool for isolating the effect of specific point defect/sink reactions to aid in the comparison and evaluation of the two computational models.

The results of MFRT and OKMC simulations for these conditions are shown in Figs. 3–7 for an irradiation temperature of 373 K and an NRT displacement rate of 4×10^{-7} dpa/s. The dose dependence of the vacancy concentration is shown in Fig. 3, where the expected influence of the various sink structures can be seen. There is initially little difference between the biased and unbiased interstitial clusters cases when point defect clusters are the only sink; the difference increases at higher doses when the cluster sink strength increases. The addition of a biased dislocation sink increases the vacancy concentration at the lowest doses due to increased partitioning of vacancies and interstitials, but the concentration is reduced at higher doses due to a higher overall sink strength.

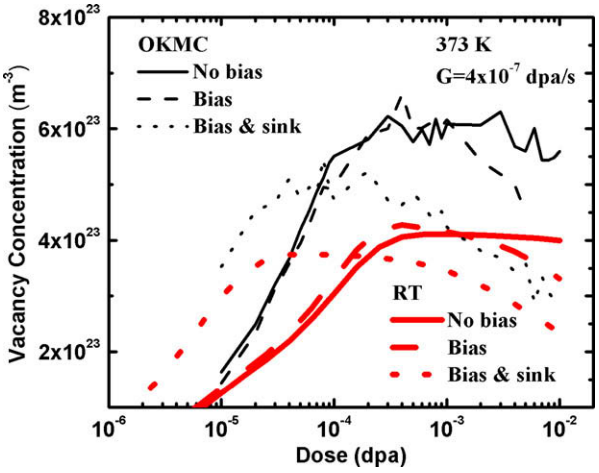

Fig. 3. Vacancy concentration for the case of only Frenkel pair production and three sink variants (see text).

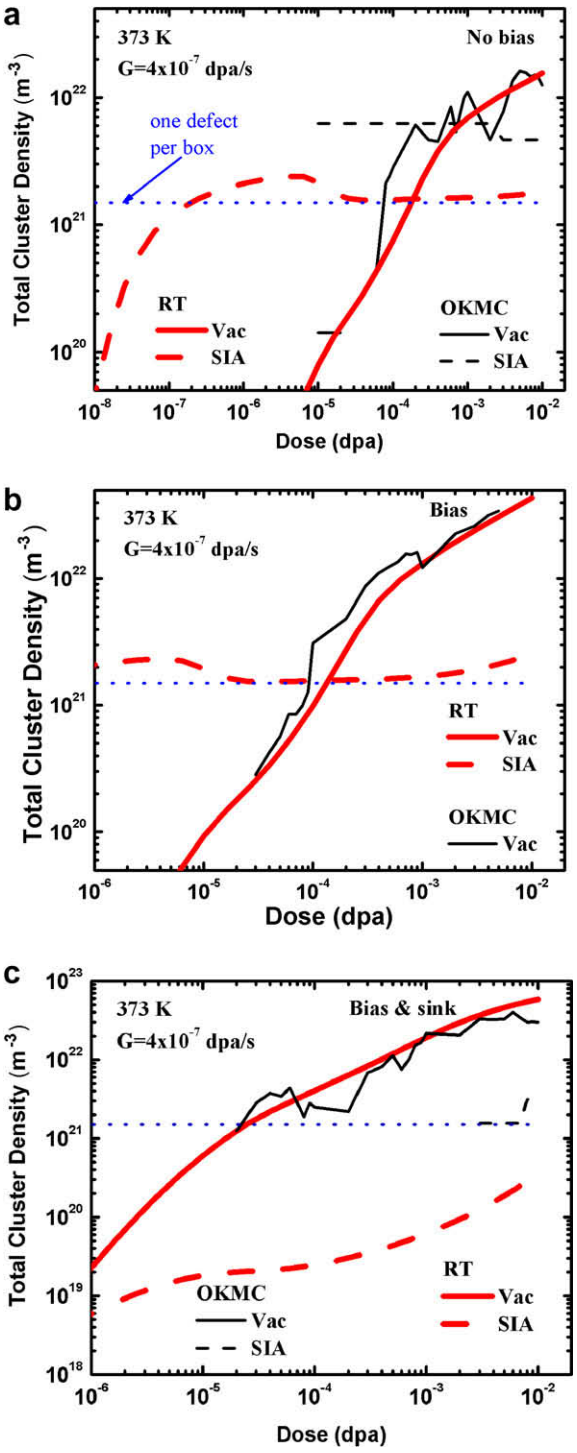

Fig. 4. Dose dependence of vacancy and interstitial cluster density predicted by MFRT and OKMC for three types of sink structures: (a) only point defect clusters, no biased absorption; (b) same as (a) but interstitial clusters have 20% bias for SIA; and (c) same as (b) but add fixed dislocation density with 20% bias for SIA.

Although the trends are similar in both the OKMC and MFRT results, the vacancy concentration is consistently higher in the OKMC simulations. This difference arises as a result of the differences in the point defect cluster sink strength discussed above and illustrated in Fig. 2. The lattice-based sink strength obtained with the OKMC is smaller than that from the continuum MFRT model in

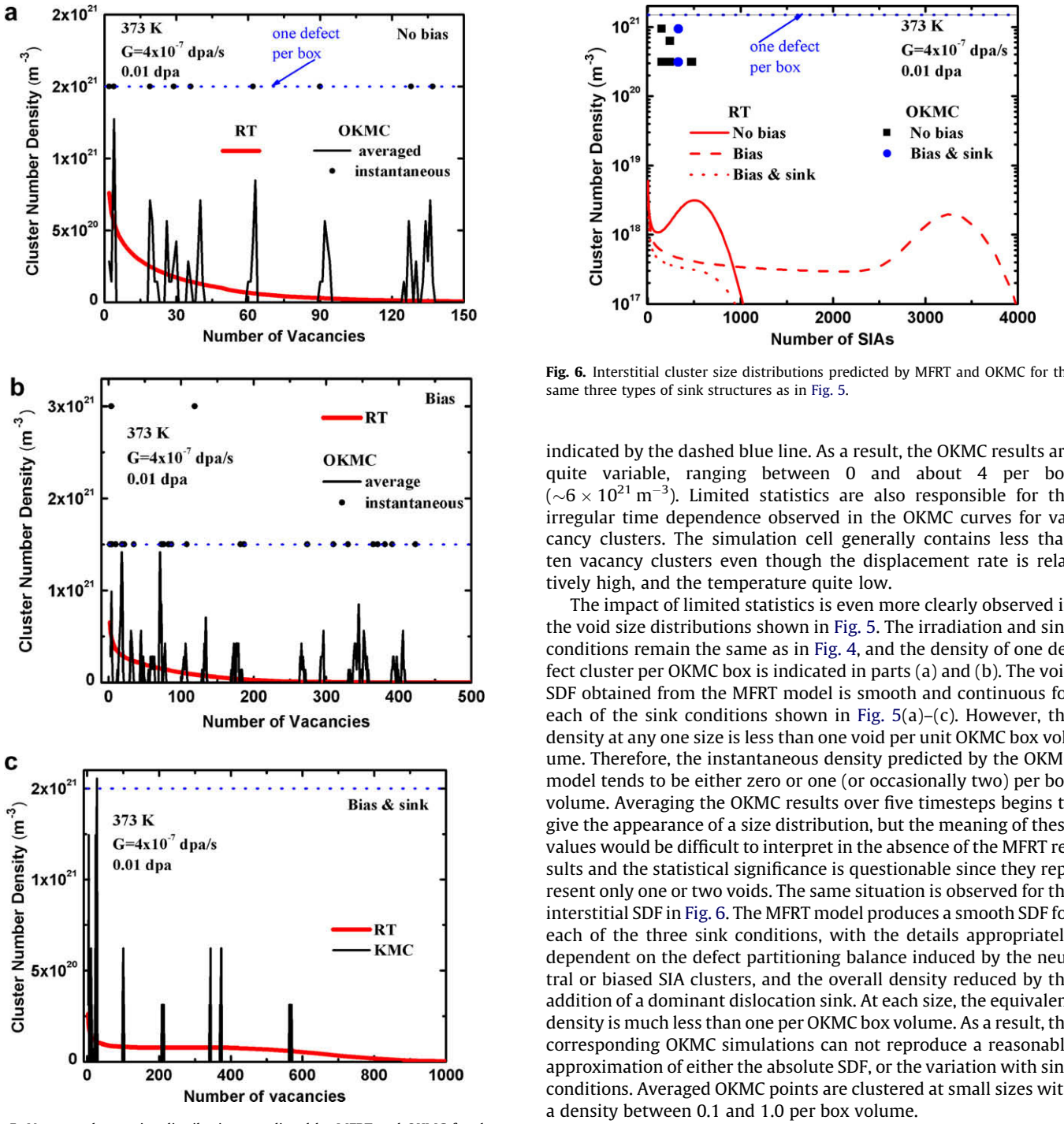

Fig. 5. Vacancy cluster size distributions predicted by MFRT and OKMC for three types of sink structures: (a) only point defect clusters, no biased absorption; (b) same as (a) but interstitial clusters have 20% bias for SIA; and (c) same as (b) but add fixed dislocation density with 20% bias for SIA.

Fig. 6. Interstitial cluster size distributions predicted by MFRT and OKMC for the same three types of sink structures as in Fig. 5.

the size range of most of the clusters that are generated. This reduced sink strength leads to a higher concentration of free vacancies. Note that difference between the two methods is reduced when the dislocation sink is added because the significance of the cluster sink strength is reduced in this case.

The dose dependence of the vacancy and SIA cluster densities are shown in Fig. 4 for the three sink variants. The MFRT and OKMC predictions of the vacancy clusters are in good agreement for each case. However, the MFRT results indicate that the interstitial cluster density is near or below the one defect per box value which is indicated by the dashed blue line. As a result, the OKMC results are quite variable, ranging between 0 and about 4 per box ($\sim 6 \times 10^{21}$ m^{-3}). Limited statistics are also responsible for the irregular time dependence observed in the OKMC curves for vacancy clusters. The simulation cell generally contains less than ten vacancy clusters even though the displacement rate is relatively high, and the temperature quite low.

The impact of limited statistics is even more clearly observed in the void size distributions shown in Fig. 5. The irradiation and sink conditions remain the same as in Fig. 4, and the density of one defect cluster per OKMC box is indicated in parts (a) and (b). The void SDF obtained from the MFRT model is smooth and continuous for each of the sink conditions shown in Fig. 5(a)–(c). However, the density at any one size is less than one void per unit OKMC box volume. Therefore, the instantaneous density predicted by the OKMC model tends to be either zero or one (or occasionally two) per box volume. Averaging the OKMC results over five timesteps begins to give the appearance of a size distribution, but the meaning of these values would be difficult to interpret in the absence of the MFRT results and the statistical significance is questionable since they represent only one or two voids. The same situation is observed for the interstitial SDF in Fig. 6. The MFRT model produces a smooth SDF for each of the three sink conditions, with the details appropriately dependent on the defect partitioning balance induced by the neutral or biased SIA clusters, and the overall density reduced by the addition of a dominant dislocation sink. At each size, the equivalent density is much less than one per OKMC box volume. As a result, the corresponding OKMC simulations can not reproduce a reasonable approximation of either the absolute SDF, or the variation with sink conditions. Averaged OKMC points are clustered at small sizes with a density between 0.1 and 1.0 per box volume.

The number of defects accumulated in point defect clusters is shown Fig. 7 as a function of dose for the three sink conditions. This value is significant because it represents a net change in the irradiated microstructure that can ultimately be experimentally verified. For example, volumetric swelling is directly related to accumulation of vacancies. There is good agreement between the MFRT and OKMC predictions of vacancy accumulation for all three cases, although the dose dependence of the OKMC results are irregular in Fig. 7(a) and (b) due to the vacancy cluster density being only slightly greater than the one per box value (see Fig. 4). As they should, the total number of vacancies and interstitials accumulated in clusters approach the same value as the dose increases in Fig. 7(a) and (b). SIA accumulation is also in reasonable agreement except for the third case in Fig. 7(c), where the interstitial cluster density is less than one per OKMC box volume (Fig. 4).

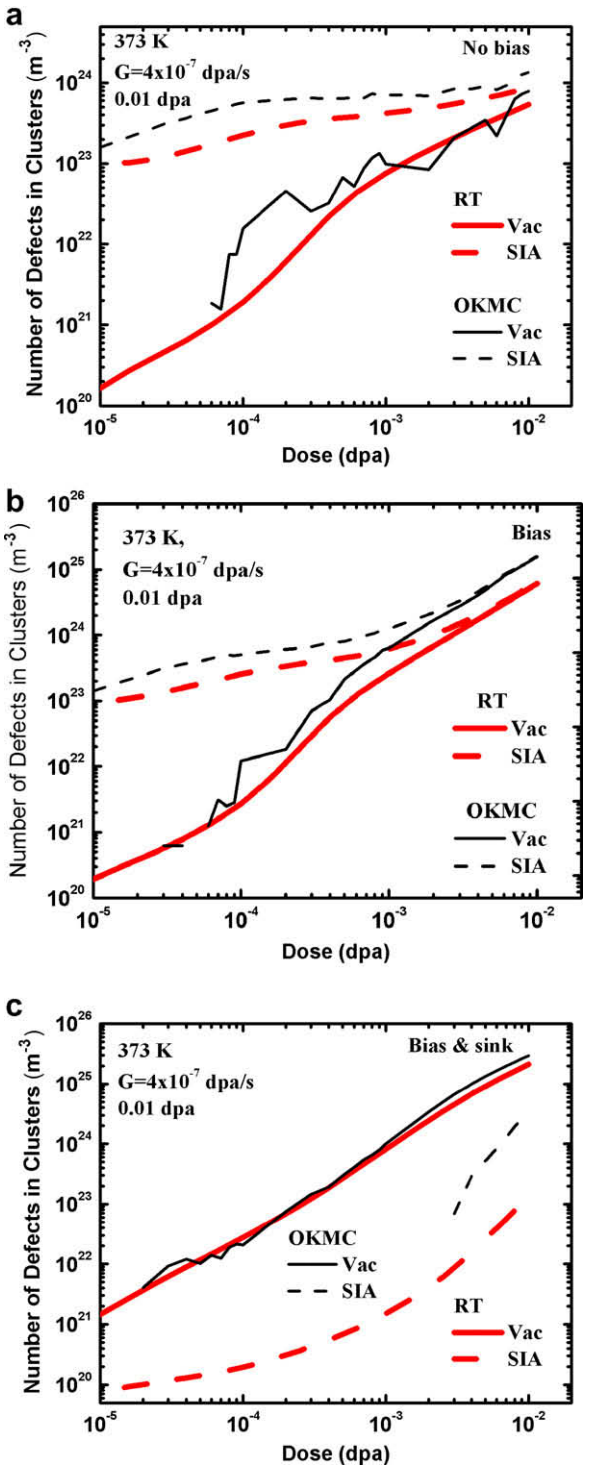

Fig. 7. Number of vacancies and interstitials accumulated in clusters predicted by MFRT and OKMC for the same three types of sink structures as in Figs. 5 and 6.

The results shown in Figs. 8 and 9 illustrate the effect of irradiation temperature at a relatively high damage rate of 4×10^{-5} dpa/s. The vacancy concentration is shown in Fig. 8(a) and the void number density in Fig. 8(b). Fig. 9(a) shows the number of vacancies accumulated in clusters, and the vacancy cluster size distribution is shown in Fig. 9(b) at two doses for a temperature of 100 °C. The results in Figs. 8 and 9(a) and (b) were obtained for the sink conditions that include an interstitial bias for the interstitial clusters, but no fixed sink. The fixed dislocation sink is added in Fig. 9(b). The MFRT and OKMC results are in reasonable agreement, with the vacancy concentration slightly higher for the OKMC model because of the difference in the vacancy cluster sink strength discussed above. For temperatures greater than about 200 °C, the predictions of the OKMC model show considerable scatter due to the limited number of vacancies and vacancy clusters in the simulation cell. In fact, these results provide a useful measure of the number of objects required for the OKMC model to provide an adequate representation of the MFRT results. For example, in Fig. 8(a), there is considerable scatter in the value of the vacancy concentration obtained from the OKMC model at 250 °C. At this temperature, the number of vacancies in the simulation cell is about 100. At the higher temperature of 300 °C, where there are about 50 vacancies in the simulation cell, the scatter in the vacancy concentration is ±50%. The vacancy cluster number density falls below one per OKMC cell volume for temperatures greater than 200 °C. The conditions for the size distribution comparison shown in Fig. 9(b) were chosen to have a high cluster density, that is, $T = 100$ °C and with the biased dislocation sink included. For this case, the MFRT and OKMC predictions are similar at both 0.005 and 0.01 dpa.

Figs. 10–12 illustrate the impact of atomic displacement rate at a temperature of 100 °C. Results are shown for three displacement rates, 4×10^{-7}, 4×10^{-6}, and 4×10^{-5} dpa/s. Values of the vacancy concentration obtained from the two models are in good agreement at each damage rate. However, even at these relatively high displacement rates, the interstitial concentration remains well below the density, which is equivalent to one object in the OKMC simulation cell. Therefore, it is not possible to obtain an accurate value for the interstitial concentration from the OKMC model. This point is further demonstrated by the point defect cluster densities shown in Fig. 11. Although the two models predict similar values for the void density, substantial fluctuations are observed in the OKMC results as long as the number of voids in the simulation cell is less than a few hundred. Only for the highest displacement rate of 4×10^{-5} dpa/s is the number of interstitial clusters in the OKMC cell greater than one. Similarly, Fig. 12 indicates that it is only at this very high displacement rate that the void size distribution function obtained from the OKMC contains enough objects to give a good representation of the SDF obtained from the MFRT (Fig. 12(c)).

The two sets of simulations involving cascade damage conditions are summarized in Figs. 13–16. The conditions chosen for this comparison were an NRT displacement rate of 1×10^{-5} dpa/s, cascade efficiency of 0.4, temperature of 200 °C, and with the most complete sink structure. The cascades used in the OKMC simulations shown in Figs. 13 and 14 are what might be termed realistic cascades, that is, the spatial correlation of the point defects and small clusters is typical of a cascade obtained from molecular dynamics simulations. This spatial correlation was removed in the 'cascades' used to obtain the OKMC results shown in Figs. 15 and 16. The same MFRT predictions are used for comparison in both cases.

Although in-cascade production of point defect clusters increases the cluster density, raising the temperature to 200 °C reduces the point defect concentrations. As a result, the agreement between the OKMC and MFRT is relatively poor for the vacancy concentration in Fig. 13(a); and the interstitial density is too low to be accurately modeled using OKMC. Values for the total point defect cluster densities are in relatively good agreement in Fig. 13(b) because a sufficiently large number of clusters are formed, particularly for voids. Similarly, the number of vacancies and interstitials accumulated in clusters is in fair agreement as seen in Fig. 14(a). However, an additional discrepancy between the MFRT and OKMC results exists. The number of interstitials accumulated in SIA clusters should approach the number of vacancies in voids at the higher doses, with a slight excess in vacancy

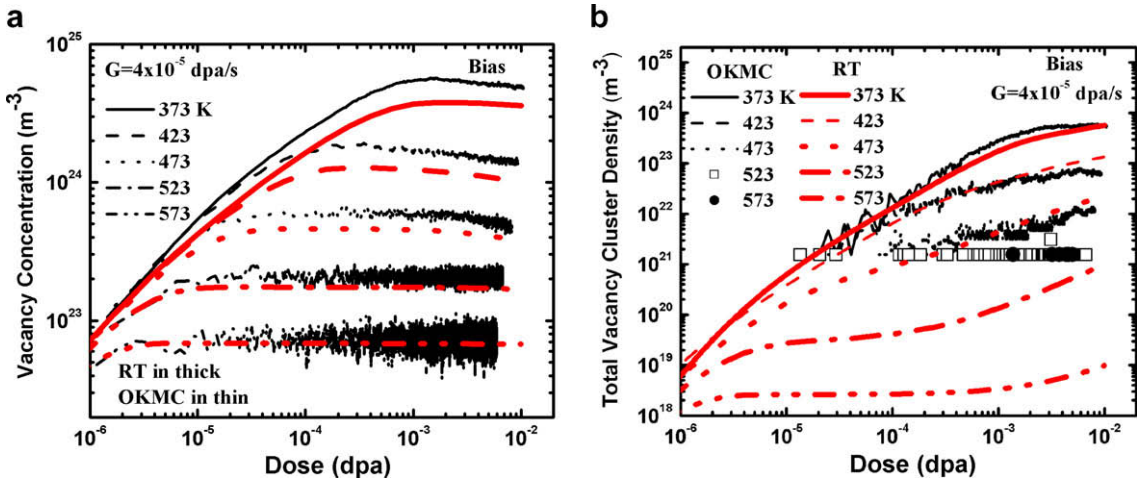

Fig. 8. Influence of irradiation temperature on MFRT and OKMC predictions of (a) vacancy concentration and (b) vacancy cluster density.

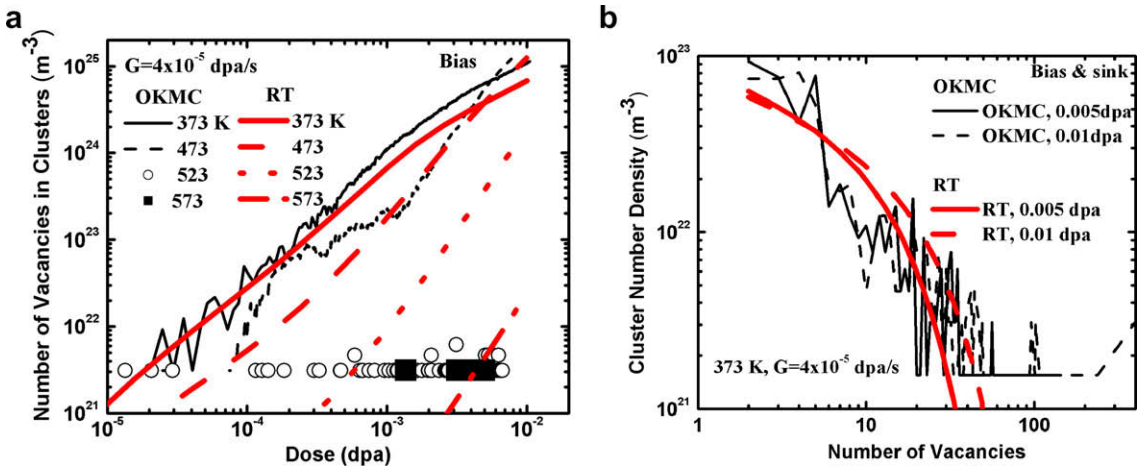

Fig. 9. Influence of irradiation temperature on MFRT and OKMC predictions of (a) vacancies accumulated in clusters and (b) vacancy cluster size distribution.

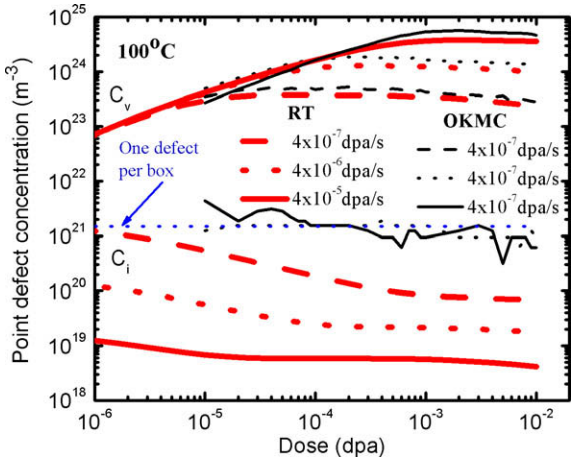

Fig. 10. Influence of atomic displacement rate on point defect concentrations predicted by MFRT and OKMC at 100 °C.

accumulation due to the dislocation-interstitial bias. This is the case for the MFRT curves in Fig. 14(a), but the vacancy and interstitial curves are diverging for the OKMC model. Moreover, an excess interstitial accumulation is observed for the OKMC case. This difference between the two models can be understood by referring to the cluster size distributions shown in Fig. 14(b). The MFRT and OKMC results are in fair agreement only at small sizes where a large number of clusters exist. However, the OKMC model can not produce the smooth distribution seen in the MFRT predictions at larger sizes because the density of large clusters is too low. Although the total number of clusters of both types exceeds the one per box volume criterion (Fig. 13(b)), the number at any given size is much lower. Spurious formation of large SIA and vacancy clusters results from the fluctuations in the OKMC results, and this leads to the higher level of accumulation predicted by the OKMC model shown in Fig. 14(a). The discrepancy is greater for the SIA clusters because the MFRT model indicates that the cluster density should be essentially zero for SIA clusters larger than about 75.

Although the simulated cascades used in the OKMC model to produce the results shown in Figs. 15 and 16 are less representative of real atomic displacement cascades, they provide a better simulation of how primary damage production is modeled in the MFRT. Therefore, it is not surprising that the agreement between the two models is somewhat improved for this case, which can be confirmed by a careful comparison of Fig. 13 with Fig. 15 and Fig. 14 with Fig. 16. Recall that the red MFRT curves are the same in both sets of figures. For example, the OKMC vacancy cluster density in Fig. 15(b) is closer to the MFRT result than the corresponding curve in Fig. 13(b), and the agreement for the number of vacancies in clusters is improved between Figs. 14(a) and 16(a). The excess interstitial accumulation observed for the OKMC model in Fig. 14(a) is somewhat worse with the 'random' cascades in

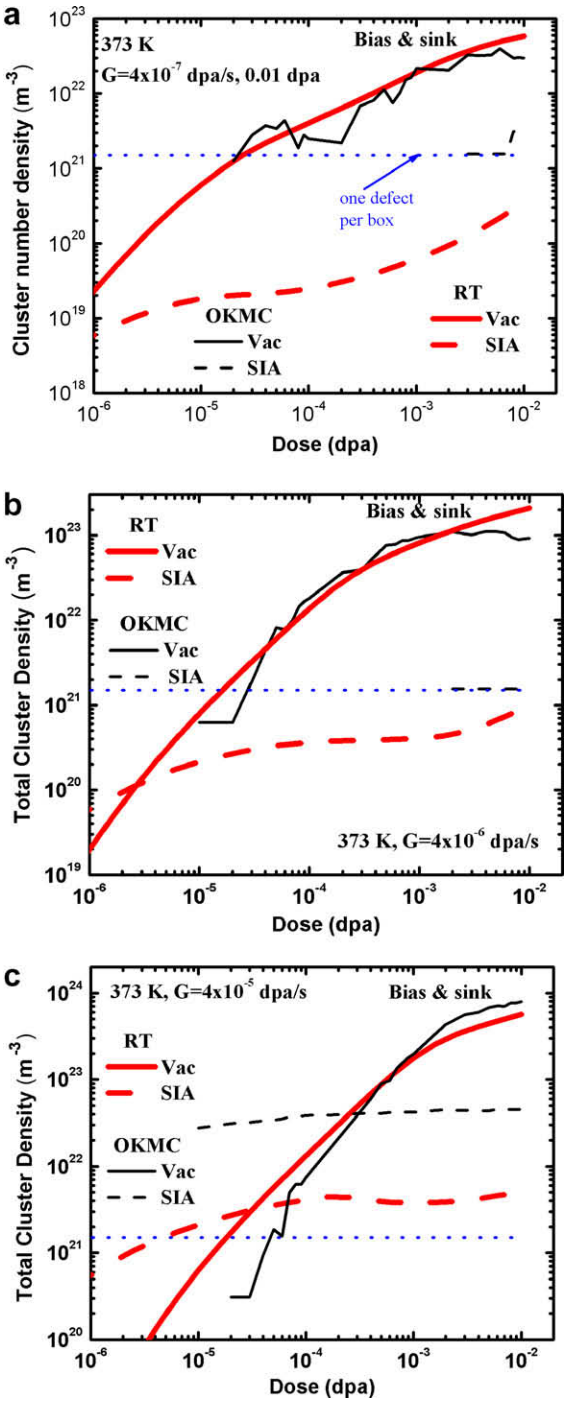

Fig. 11. Influence of atomic displacement rate on MFRT and OKMC predictions of vacancy and SIA cluster density at 100 °C for three types of sink structures: (a) only point defect clusters, no biased absorption; (b) same as (a) but interstitial clusters have 20% bias for SIA; and (c) same as (b) but add fixed dislocation density with 20% bias for SIA.

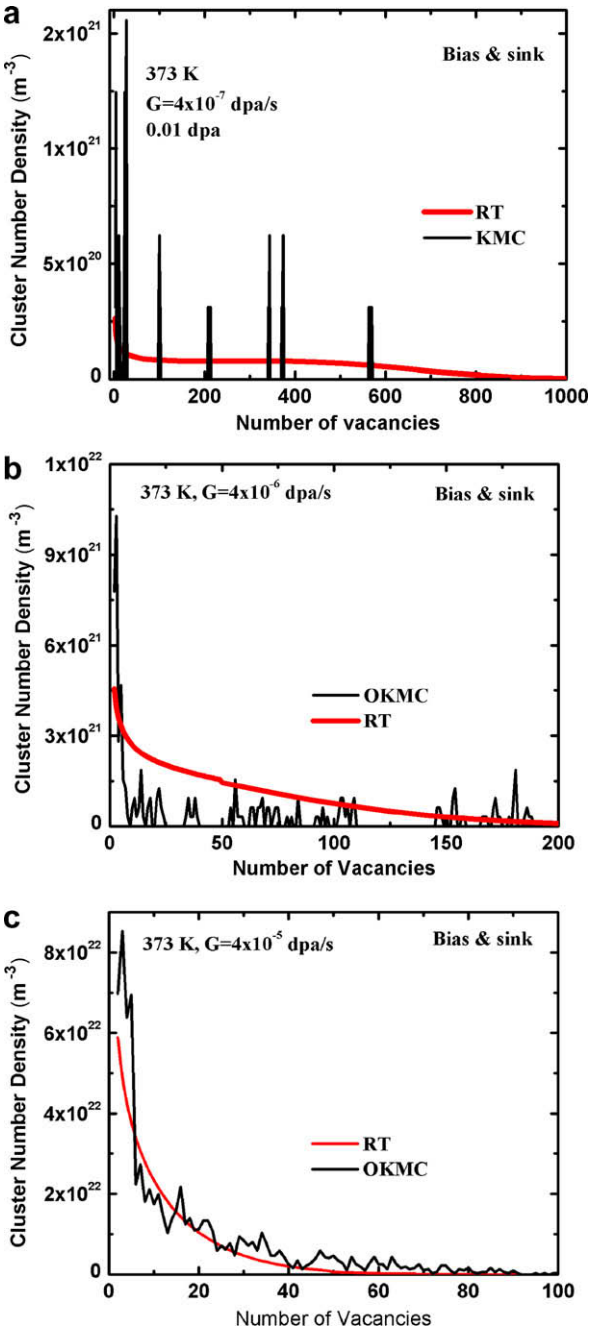

Fig. 12. Influence of atomic displacement rate on MFRT and OKMC predictions of vacancy cluster size distribution at 100 °C for the same three types of sink structures as in Fig. 11.

Fig. 16(a), largely due the improvement (reduction) in the number of vacancies in clusters. There is little improvement in the vacancy concentration (Figs. 13(a) vs. 15(a)), no doubt due to the limited statistics in the OKMC results.

4. Discussion

The results presented in the preceding section have highlighted both the similarities and differences inherent in the reaction MFRT and OKMC methods. They confirm that the two methods will give nearly identical results if the problem to be solved is well posed. However, because of the inherent differences in the methods listed in Table 1 and discussed above, specifying the problem in such a way as to obtain the desired equivalence is not a trivial exercise. For example, if small point defect clusters are described in a 'standard' way in both approaches, the inherent difference between the OKMC lattice-based reaction rates and the MFRT continuum sink strengths will lead to a systematic difference in the results. The OKMC reaction rates lead to a lower effective sink strength, which increases the concentration of mono-defects in the matrix. The significance of this difference depends on the details of the problem. It is greater for conditions in which small defect clusters are more

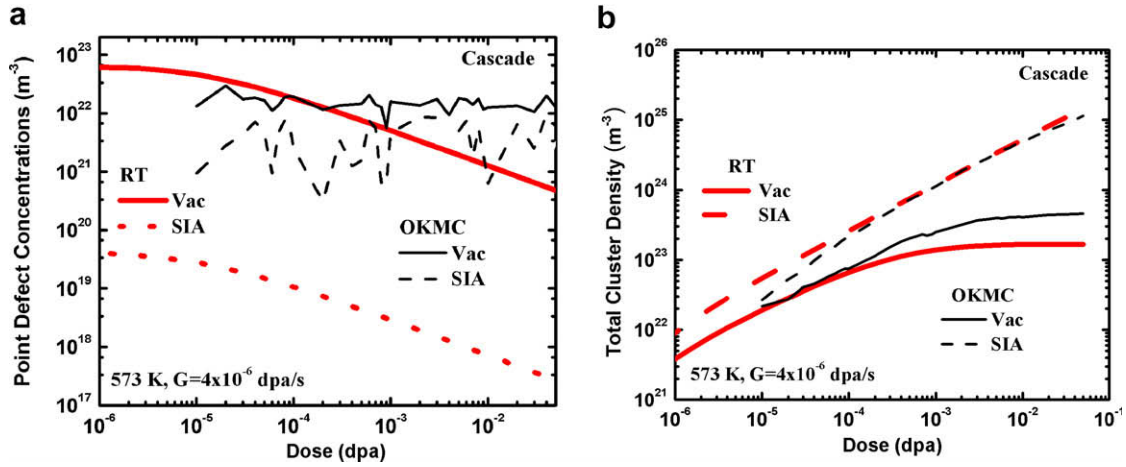

Fig. 13. Dose dependence of MFRT and OKMC predictions of (a) point defect concentrations and (b) point defect cluster densities, under cascade damage production with interstitial-biased SIA clusters and fixed dislocation sink. Dashed blue lines indicate one defect in OKMC box.

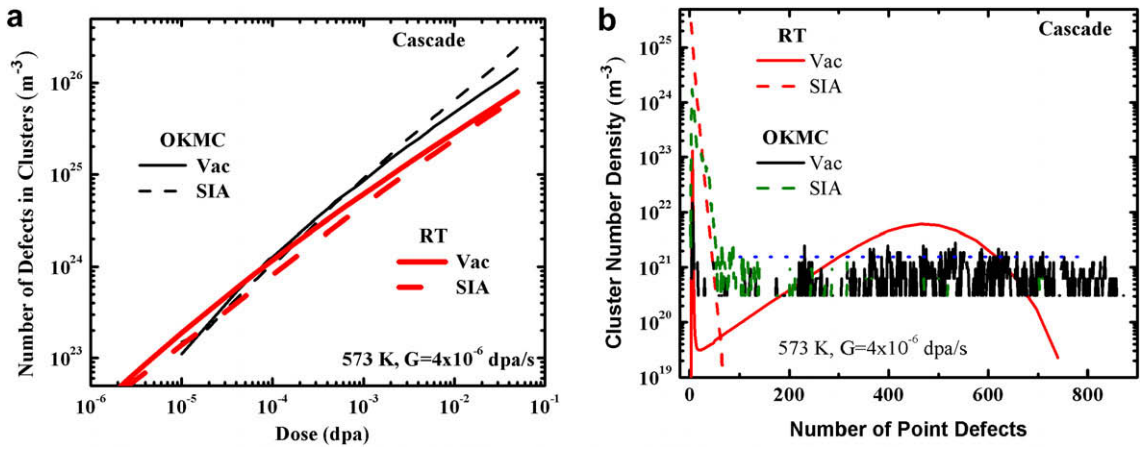

Fig. 14. MFRT and OKMC predictions of (a) point defects accumulated in clusters and (b) cluster size distributions, under cascade damage production with interstitial-biased SIA clusters and fixed dislocation sink. Dashed blue line in (b) indicates one defect in OKMC box.

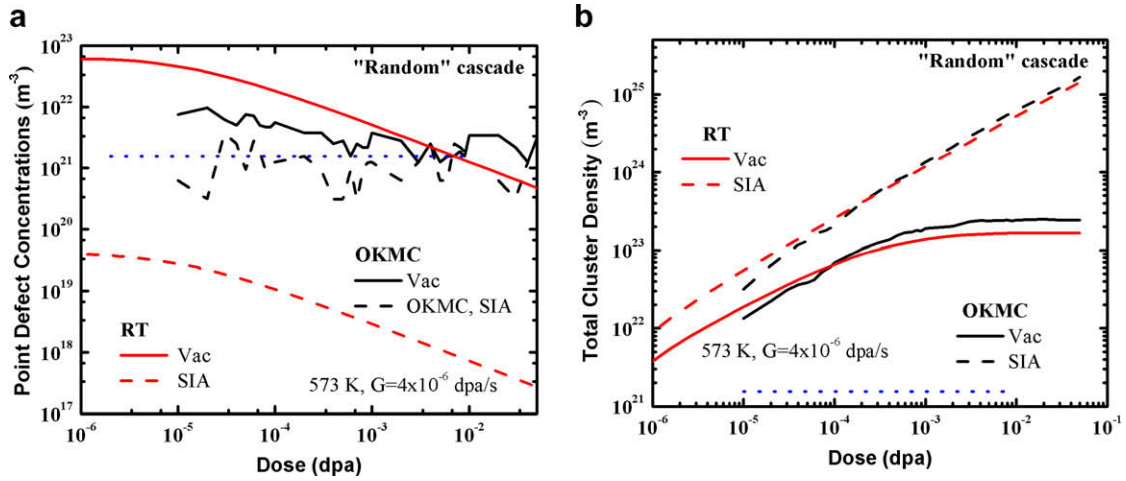

Fig. 15. Dose dependence of MFRT and OKMC predictions of (a) point defect concentrations and (b) point defect cluster densities. Cascade damage production in which defects have no spatial correlation, sink structure as in Figs. 13 and 14. Dashed blue lines indicate one defect in OKMC box.

dominant, for example, electron irradiation of a material with a low dislocation density. Lower temperatures and higher damage rates would also increase its significance.

It may be argued that the OKMC reaction rates are more accurate for the small clusters because a collection of only a few vacancies may be poorly described by the spherical approximation used

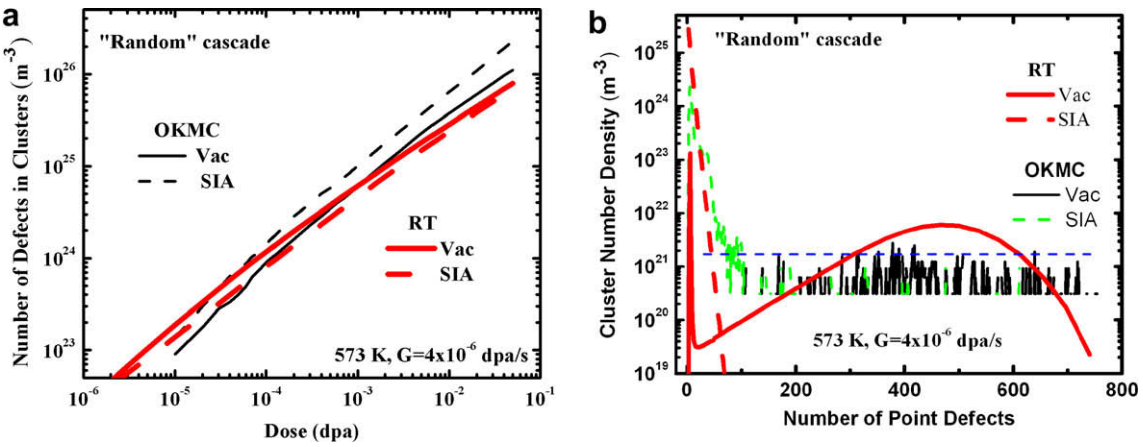

Fig. 16. MFRT and OKMC predictions of (a) point defects accumulated in clusters and (b) cluster size distributions. Cascade damage production in which defects have no spatial correlation, sink structure as in Figs. 13 and 14. Horizontal dashed blue line in (b) indicates one defect in OKMC box.

in the MFRT sink strengths. Similarly, the ability to accurately include the spatial correlation of the defects produced by displacement cascades is an advantage of the OKMC relative to the MFRT. These differences could be accounted for in the MFRT by using the results of specifically designed OKMC simulations to provide a set of correction factors that could be applied in the MFRT models. For example, information such as that shown in Fig. 2 could be used to correct the MFRT sink strengths for small point defect clusters. Monte Carlo simulations could also be used to determine the degree of additional point defect recombination that occurs due to spatial correlations in-cascade debris [16], and a correction could be applied to the MFRT damage production rate.

The primary limitations of the OKMC model are related to computational issues. Even with modern computers, the maximum simulation cell size and the maximum dose (typically much less than 1 dpa) that can be simulated are limited. Increasing either of these parameters necessitates a reduction in the other. The limited cell size directly specifies the minimum density of any type of object in the system; no density lower than one object per simulation cell volume can be simulated. Because defect densities are a strong function of irradiation temperature and damage rate, the density limit implies limits on the irradiation conditions that can be simulated. For a given box size, there will be a combination of maximum temperature and minimum dose rate for which the OKMC model can be used. However, an object density of one per box volume is not a sufficient criterion for successful use of the OKMC. Because of the statistical nature of Monte Carlo methods, there should be enough objects of each type to ensure the statistical significance of the results. The results shown in Fig. 8(a) provide the clearest example. Significant fluctuations in the vacancy concentration were observed even when there were as many as 300 vacancies in the simulation cell, partly because there were less than 10 vacancy clusters to act as sinks. Under conditions in which nucleation of extended defects is difficult and proceeds primarily on the basis of true fluctuations (high temperature and low damage rate), the OKMC method is unlikely to predict accurate nucleation rates if a statistically significant number of the nucleating species is not present (see the discussion related to Figs. 13–16).

In contrast with the OKMC, even very detailed MFRT models can simulate microstructural evolution for doses up 100 dpa or greater in clock times that are relatively short. Within the context of the effective medium, essentially any defect density can be simulated. Overall, the agreement between the two methods is best for irradiation conditions that produce a high density of defects (lower temperature and higher displacement rate) and for materials that have a relatively high density of fixed sinks such as dislocations. The higher dislocation density reduces the significance of differences associated with the sink strength of small defect clusters and differences that may arise between the number of point defect clusters that are formed.

5. Summary

This study has verified the ability of alternate approaches based on the reaction rate theory, MFRT and OKMC to obtain comparable results in well-posed simulations that are directly relevant to modeling radiation-induced microstructural evolution. It has also helped to define irradiation regimes in which it may be inappropriate to use the OKMC methods. In particular, current computational limitations on the OKMC simulation cell size imply that it may be difficult to use the OKMC to simulate some aspects of microstructural evolution at the modest displacement rates and elevated temperatures relevant to many reactor components. Expected advances in computing will expand the range of use for OKMC models, but this progress may occur slowly because orders of magnitude in defect density are required. However, the OKMC does a better job of accounting for spatial correlations which can influence point defect reaction rates with small defect clusters and that modify the primary damage source term under cascade damage conditions. As such, one immediate application of OKMC simulations is to improve the parameterization of the MFRT models.

Both MFRT and OKMC models have been used elsewhere to make direct, apparently successful comparisons with experimental data. However, such comparisons can be misleading because both models include a number of adjustable material parameters that may be exploited to obtain agreement. A more rigorous test of the models would involve mutual benchmarking on sample problems such as those presented here to establish model parameters, and then to simulate the desired experiments without further parameter adjustment.

Acknowledgements

The authors would like to thank Drs. L.K. Mansur, J.R. Morris, and Y.N. Osetskiy of ORNL for helpful discussion and reviews. Research at ORNL sponsored by the Office of Fusion Energy Sciences, US Department of Energy, under Contract DE-AC05-00OR22725 with UT-Battelle, LLC.

References

[1] L.K. Mansur, Kinetics of Nonhomogeneous Processes, Wiley-Interscience, New York, 1987. p. 377.
[2] M. Kiritani, J. Phys. Soc. Jpn. 35 (1973) 95.

[3] J.L. Katz, H. Wiedersich, J. Chem. Phys. 55 (1973) 1414.
[4] N.M. Ghoniem, S. Sharafat, J. Nucl. Mater. 92 (1980) 121.
[5] S.I. Golubov, A.M. Ovcharenko, A.V. Barashev, B.N. Singh, Philos. Mag. A 81 (2001) 643.
[6] R.E. Stoller, G.R. Odette, A composite model of microstructural evolution in austenitic stainless steel under fast neutron irradiation, in: F.A. Garner, N.H. Packan, A.S. Kumar (Eds.), Radiation-Induced Changes in Microstructure, ASTM STP 955, ASTM International, West Conshohocken, PA, 1987, p. 371.
[7] M.P. Surh, J.B. Sturgeon, W.G. Wolfer, J. Nucl. Mater. 325 (2004) 44.
[8] N. Metropolis, A.W. Rosenbluth, M.N. Rosenbluth, A.H. Teller, E. Teller, J. Chem. Phys. 21 (1953) 1087.
[9] W.A. Coghlan, L.K. Mansur, J. Nucl. Mater. 108&109 (1982) 246.
[10] S.I. Golubov, Phys. Met. Metallogr. (USSR) 52 (1981) 86.
[11] C. Domain, C.S. Becquart, L. Malerba, J. Nucl. Mater. 335 (2004) 121.
[12] W.M. Young, E.W. Elcock, Proc. Phys. Soc. 89 (1966) 735.
[13] B. Bortz, M.H. Kalos, J.L. Lebowitz, J. Comput. Phys. 17 (1975) 10.
[14] A.D. Brailsford, R. Bullough, Philos. Trans. Roy. Soc. Lond. A 302 (1981) 87.
[15] R.E. Stoller, A.F. Calder, J. Nucl. Mater. 283–287 (2000) 746.
[16] B.D. Wirth, G.R. Odette, R.E. Stoller, Recent progress toward an integrated multiscale-multiphysics model of reactor pressure vessel embrittlement, in: V. Bulatov, F. Cleri, L. Colombo, L. Lewis, N. Mousseau (Eds.), Advances in Materials Theory and Modeling-Bridging Over Multiple-Length and Time Scales MRS, vol. 677, Materials Research Society, Pittsburgh, Pennsylvania, 2001, p. 5.2.1.